Ecological Indicators 155 (2023) 111006

Contents lists available at ScienceDirect

Ecological Indicators

journal homepage: www.elsevier.com/locate/ecolind

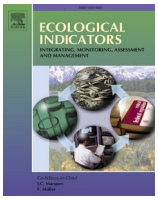

The constraint effect of grassland vegetation on soil wind erosion in Xilin Gol of China

Zeyao Li [a], Jiarong Wei [a,1], Ruifang Hao [a,b,*]

[a] Department of Physical Geography and Resources and Environment, School of Soil and Water Conservation, Beijing Forestry University, Beijing 100083, China
[b] Yanchi Research Station, School of Soil and Water Conservation, Beijing Forestry University, Beijing 100083, China

ARTICLE INFO

Keywords:
Constraint line method
Grassland
Net primary productivity
Soil erosion by wind
Thresholds

ABSTRACT

As an important part of the natural ecosystem, grassland has great significance to worldwide sustainability. The Xilin Gol grassland is the closest natural grassland to Beijing, the wind and sand conditions there can have a direct impact on Beijing's ecological environment. This study estimated the net primary productivity (NPP) and soil erosion by wind (SL) from 2001 to 2014 in the Xilin Gol League, and 10 equally spaced constraint lines from 10 % to 99.99 % quantile of NPP-SL scatter cloud were extracted for each year. We also analyzed the eigenvalues of these constraint lines. The results showed that the soil wind erosion of nearly half area of the Xilin Gol was concentrated in the range of 0–5 kg/m^2, where SL was more constrained by non-vegetation factors than NPP from 2001 to 2014. The occurrence of the threshold values for the 60 %-90 % quantile constraint lines in the Xilin Gol grassland was more frequent at NPP levels of 250 gC/m^2 and 400 gC/m^2. And there was a "constraint bottleneck" between 300 gC/m^2 and 400 gC/m^2 at the middle steady part of the S-shaped constraint lines, where SL remained relatively stable with the increasing NPP. This study not only broadens the application of the constraint line method in ecology, but also helps to deeply and comprehensively demonstrate the constraint effect of grassland vegetation on soil wind erosion in complex ecosystems, which contributes to regional sustainability.

1. Introduction

Grassland is a widely distributed vegetation type, covering approximately 23 % – 25 % of the world's total area (Kang et al., 2007). The grassland ecosystem can regulate climate, conserve the source of water, protect water and soil, and prevent wind, and it is also an important place for the development of animal husbandry (Hou et al., 2021). In this way, the grassland ecosystem is of great significance to the maintaining of the natural ecosystem pattern (Bengtsson et al., 2019). However, grassland has been degenerating all over the world because of some natural and human factors such as climate change and overgrazing (Akiyama and Kawamura, 2007). The deterioration of grassland has led to a series of ecological problems, for example, soil erosion by wind. Soil erosion by wind can cause dust pollution and sandstorms in and around the area, which have a negative impact on the human living environment and endanger human health (Tian et al., 2021).

It has long been recognized that vegetation can prevent wind erosion through multiple ways (Gibbens et al., 1983; Siddoway et al., 1965; Yan et al., 2011). Numerous studies have been carried out on the internal mechanism between vegetation and soil erosion by wind, such as acting as a physical barrier, stabilizing soil structure with root systems, intercepting wind energy, promoting the accumulation of organic matter, and increasing surface roughness (Han et al., 2023; Li et al., 2018; Zhang et al., 2022). Early studies were usually conducted by way of field trips. For instance, wind tunnel testing was used to determine the critical values of different vegetation coverage to resist wind erosion (Hu et al., 1991). The influence of vegetation characteristics on soil erosion has been studied through a fixed-point field investigation (Shang et al., 2006). As the development and application of remote sensing technology, Geographic Information System (GIS) and computer analog technology (Ali et al., 2016; Liu et al., 2010), related studies have entered a new stage of large scale and digitalization (Gong et al., 2014b; Wang et al., 2020; Zhang et al., 2021).

Furthermore, the constrain line method has been introduced to study the constraint effect between vegetation and soil erosion by wind because of its advantages in describing the complex ecological process

* Corresponding author at: School of Soil and Water Conservation, Beijing Forestry University, No. 35, Qinghua East Road, Haidian District, Beijing 100083, China.
E-mail addresses: yaoyao26788ok@bjfu.edu.cn (Z. Li), weijr@bjfu.edu.cn (J. Wei), hrf@mail.bnu.edu.cn (R. Hao).
[1] Co-first author.

https://doi.org/10.1016/j.ecolind.2023.111006
Received 4 June 2023; Received in revised form 21 September 2023; Accepted 24 September 2023
Available online 29 September 2023

affected by multiple factors (Hao et al., 2016). A conclusion has been researched by analyzing the constraint line of net primary productivity (NPP) and soil erosion by wind (SL) that the constraint effect of crops on soil wind erosion control is weaker than that of forest and grassland vegetation (Hao et al., 2017). The vegetation coverage does not have positive effect on soil wind erosion if it is less than 20 %, while the soil wind erosion almost disappears if it is higher than 60 % (Zhao et al., 2017b). However, most of these former studies obtained constraint lines by fitting the boundary points of scatter clouds, which can only describe the case when the effect of other influencing factors is minimal. Nevertheless, in reality, it is impossible for this case because of the complex ecological processes involved. Therefore, a deep and comprehensive study of the relationship between NPP and SL is highly necessary.

The Xilin Gol League in Inner Mongolia is one of the regions with the most homogeneous land use type of grassland in China. The grassland coverage rate reaches more than 80 %. The unreasonable exploitation of grasslands in the past has caused the degradation of grasslands and the soil wind erosion problem used to be quite serious in the Xilin Gol League (Sun et al., 2017). To protect the grassland ecology, large-scale ecological restoration policies have been implemented since 2000, adopting long-term measures such as The Grain for Green Program, which achieves significant improvement in the regional ecological environment. However, The Xilin Gol League is located in arid and semi-arid areas in northern China, where water yield is the main factor limiting the stability of local ecosystems. Simply increasing vegetation coverage may not effectively reduce soil wind erosion, but rather increase the pressure of the local water supply. Therefore, it is important to find an optimal vegetation condition that suppresses soil wind erosion. This study selected the Xilin Gol League as the study area and assessed NPP and SL in this area from 2001 to 2014, and drew constraint lines based on quantile points with every tenth value from 10 % to 100 % in the scatter cloud plot of NPP-SL data. The full description of scatter clouds would contribute to a deeper understanding of the constraining of the different vegetation condition on soil wind erosion. The main objectives of this study are to 1) quantify the constraint effect of NPP on SL in Xilin Gol League, and identify key features on the constraint lines, 2) discuss the method of extracting ecological information underlying the scatter clouds to enrich the understanding of the relationship between NPP and SL, 3) provide the ecological restoration and sand control projects with theoretical foundation to promote regional sustainability.

2. Materials and methods

2.1. Study area

The Xilin Gol League has an area of 202,580 km^2 (Fig. 1). The geographical location is 42°32′-46°41′N and 111°59′-119°58′E. The topography of the region is predominantly high plateau, with an elevation of 760–1960 m, an average elevation above 1000 m, and a southern high and northern low terrain (Hui et al., 2022). The zonal vegetation is grassland, including the typical grassland, meadow grassland, and desert grassland. The region has a typical temperate arid semi-arid continental climate, characterized by aridity, coldness, and strong winds. The average annual temperature ranges from 0℃ to 3℃, and the average annual precipitation is about 295 mm. The precipitation decreases from southeast to northwest, while the evaporation increases (Hui et al., 2022). Due to the blocking effect of the mountains, the prevailing westerly winds cause strong erosion on the surface soil from March to May, when wind speeds can reach 10.8 m per second or higher. Together with the synchronous rainfall, heat, and light, the flat terrain and abundant grassland resources provide favorable natural conditions for the development of animal husbandry. Facing the dual pressures of climate change and human activities, the regional vegetation had once undergone extensive degradation. China has implemented the policy of grassland restoration and returning farmland to forest and grass over 20 years, and 74.8 % of local grasslands were improved (Shao et al., 2017).

2.2. Estimation of net primary productivity

NPP can directly characterize the productive capacity of plant

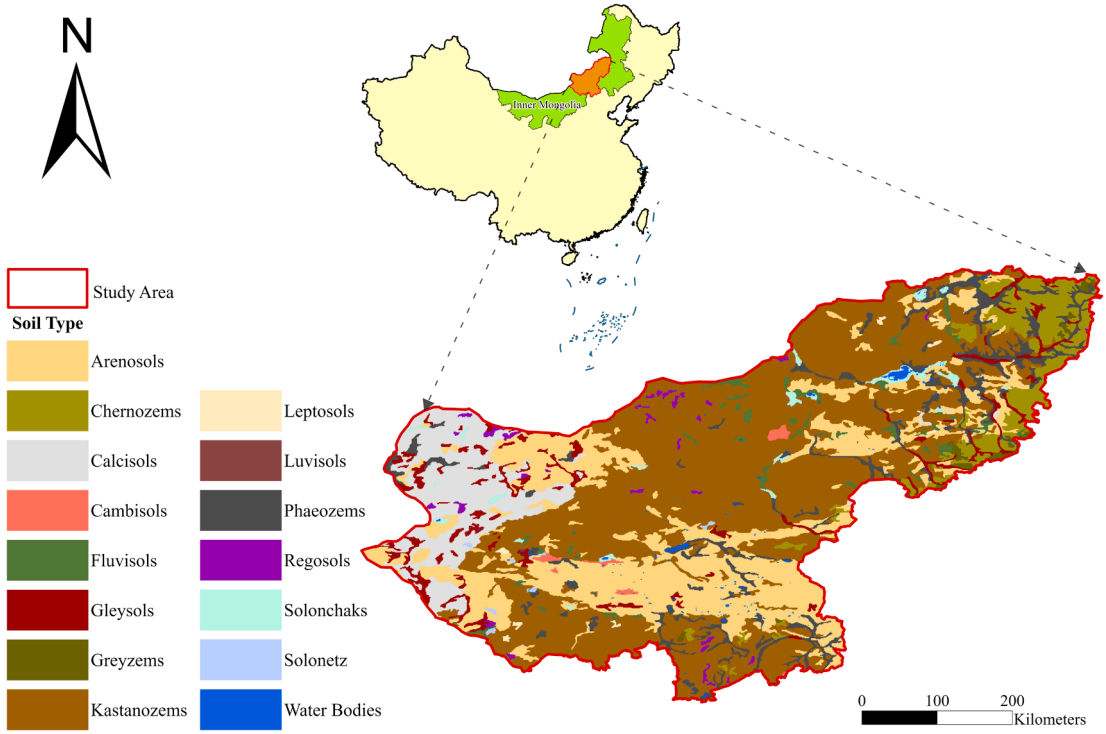

Fig. 1. The location of the Xilin Gol League.

communities under natural environmental conditions and is an important variable reflecting vegetation vitality (Zhang et al., 2016). In this study, NPP was estimated using the Carnegie-Ames- Stanford Approach (Potter et al., 1993). The model is expressed as follows:

$$NPP = F(SOL \times NDVI) \times \varepsilon \quad (1)$$

where *NPP* represents the monthly net primary productivity (gC/m^2); *SOL* represents the total solar radiation (MJ/m^2) calculated based on the daily sunshine duration; *NDVI* represents the normalized difference vegetation index derived from Moderate Resolution Imaging Spectroradiometer data; and ε represents the light utility efficiency determined by temperature and precipitation (Zhu et al., 2007).

Table 1 provides a brief description of the datasets used. All datasets were resampled or spatially interpolated to a spatial resolution of 250 m before being entered into the estimation model.

2.3. Estimation of soil erosion by wind

The Revised Wind Erosion Equation has the advantages of comprehensive consideration of multiple factors including climate and surface, as well as the convenience of data acquisition. It has been effectively applied in the estimation of grassland wind erosion in Northern China (Gong et al., 2014a; Guo et al., 2013). Thus, we used the Revised Wind Erosion Equation to estimate the soil wind erosion in this study. The model is expressed as follows:

$$Q_{\max} = 109.8 \times WF \times EF \times SCF \times K \times COG \quad (2)$$

$$s = 150.71 \times (WF \times EF \times SCF \times K \times COG)^{-0.3711} \quad (3)$$

Table 1
Description of the study data.

Data	Data description	Date source
Climate data	Daily mean temperature	Meteorological Sharing Service System in China
	Daily maximum temperature	
	Daily minimum temperature	
	Daily rainfall	
	Daily mean wind speed	
	Daily sunshine duration	
DEM	Digital Elevation Model with 90 m spatial resolution	Geospatial Data Cloud, Computer Network Information Center, Chinese Academy of Sciences
Soil data	Soil texture, topsoil sand fraction, topsoil silt fraction, topsoil clay fraction, topsoil organic carbon with 1 km spatial resolution	Cold and Arid Regions Science Data Center at Lanzhou
Land use/cover	Land use/cover with 1 km spatial resolution in 2000, 2005, 2010, and 2015	Infrastructure of Earth System Science
Normalized Difference Vegetation Index (NDVI)	Monthly NDVI with 1 km spatial resolution in 2000	Geospatial Data Cloud, Computer Network Information Center, Chinese Academy of Sciences
Soil roughness	The soil roughness for different land use/cover types	(Fryrear et al., 1998; Gong et al., 2014b)
Crop barrier	The optical density and stand density of forest areas in 2000, 2005, 2010, and 2015	(Fryrear et al., 1998)

$$SL = 2x/s^2 Q_{max} exp\left(-(x/s)^2\right) \quad (4)$$

where Q_{max} refers to the maximum transport capacity calculated based on the climate factor (WF), the soil erodibility factor (*EF*), the soil crust factor (*SCF*), soil roughness (*K*), and combined vegetation factor (*COG*); *s* represents the length of the critical field; *x* refers to the distance to the upwind edge of the field; and *SL* is the semi-monthly soil loss (kg/m^2) in the special case where Q_{max} and *s* are constant (i.e., not a function of *x*).

2.4. Constraint line method

In complex ecological ecosystems, the relationship between two variables in a bivariate scatter plot often exhibits a distribution pattern like scatter clouds (Guo and Rundel, 1998; Hao et al., 2017; Hao et al., 2016). Informative edges in the scatter clouds are referred to boundary lines. The points on the boundary line indicate that the response variable is primarily constrained by the limiting variable and not or hardly constrained by other variables. Below the boundary, as the number and intensity of additional constraint variables increase, the distance between the data points and the boundary lines also increases. Thus, compared to focusing only on the boundary lines, the analysis of constraint lines fitted by points below the boundary lines enables the measurement of the coupling interaction of all variables that are not measured but have an effect on the response variables. The comprehensive analysis makes it a preferable choice for fully characterizing the constraint effect of different vegetation conditions on soil erosion by wind.

Currently, there are four main methods for drawing constraint lines: (1) parameter method; (2) dividing scatter cloud into size classes; (3) quantile regression; (4) segmented quantile regression method. Among these, the segmented quantile regression method is more statistically grounded. On the basis of this method, the NPP on the x-axis in the scatter plot was equally divided into 100 parts to obtain 100 columns (Fig. 2), and every tenth value within the range of 10 % to 100 % was selected as a quantile point for each part. Considering the potential influence of outliers, we selected the 99.99 % quantile within each column as the boundary point, instead of using the maximum value. Based on the shapes of the scatter clouds and the goodness of fit values (R^2), we obtained the corresponding constraint lines using MATLAB 2022a. Thus, we have 10 constraint lines for each year's scatter plot.

Based on the features of the scatter clouds, we hypothesize that there

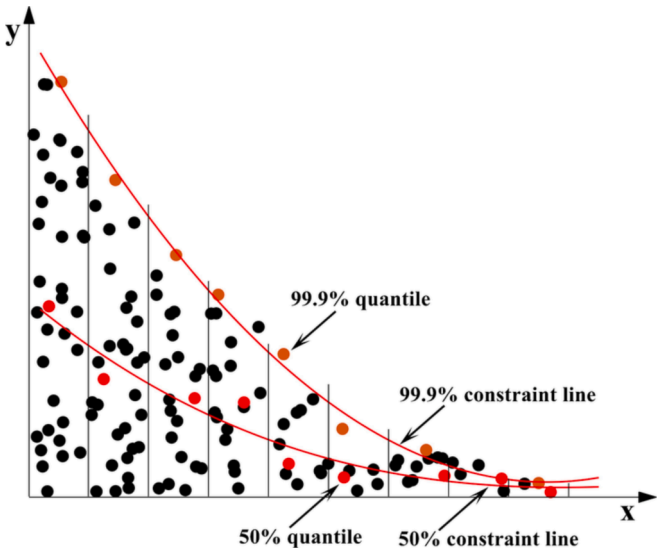

Fig. 2. Extraction of the constraint lines using the segmented quantile regression approach.

may be several types of constraint lines between NPP and SL (Fig. 3), which are: (a) Negative linear: the strength of constraint effect is constant. (b) Negative convex: the constraint effect increases gradually; (c) Backward S-shaped: over some range of NPP, there is almost no constraint effect. Over a threshold, the constraint effect sharply increases. (d) S-shaped: the constraint effect of NPP on SL can be divided into three stages: first increasing, then almost disappearing within a certain range, and finally increasing rapidly; (e) Hump-shaped: with an increase in NPP, the constraint effect first decreases and then increases. (f) concave waved: the constraint effect of NPP on SL exhibits fluctuating features.

2.5. Constraint line eigenvalue analysis method

To extract eigenvalues of different types of constraint lines accurately, we classified all constraint lines into two types, namely linear lines and non-linear lines. The slope (k) and intercept (b) of the linear constraint lines were extracted, as its mean and standard deviation were analyzed. The standard deviation divided by the absolute value of the mean was used to calculate the coefficient of variation to describe the dispersion of the data. Mori's trend analysis using the Mann-Kendall test was used to analyze the trends in the eigenvalues. The threshold values of the non-linear constraint lines were extracted as its eigenvalues to analyze the pattern of threshold occurrence. A value or interval of NPP corresponding to the higher frequency of the threshold value could guide the vegetation restoration work to achieve the maximum output of wind erosion prevention.

3. Result

3.1. Spatial and temporal variation patterns of NPP and SL

The spatial distribution of NPP and SL of the Xilin Gol League from 2001 to 2014 has obvious spatial heterogeneity (Fig. 4). In terms of multi-year average (Fig. 4(a)), the high values of NPP were concentrated in northeastern of the study area, with the highest value reaching 810.63 gC/m^2, and generally showed a trend of gradually decreasing from east to west. The spatial distribution of SL varied greatly, with the highest multi-year average reaching 46.12 kg/m^2. The areas where SL is at a higher level, the soil type is mostly arenosols (Fig. 1), while the low value areas were mainly distributed in central and peripheral of the study area. In terms of multi-year change (NPP value in 2014 minus that in 2001) (Fig. 4(b)), NPP varied greatly in space. The increase of NPP can be up to 719.37 gC/m^2, while the decrease can be as high as 53.39 gC/m^2. The areas with significant increase in NPP were mostly with low to medium multi-year average of SL. SL decreased or almost remained unchanged in most areas, with only a small part showing a significant increase.

3.2. Constraint effect of NPP on SL

There were six types of constraint lines observed, including (a) Negative linear, (b) Negative convex, (c) Backward S-shaped, (d) S-shaped, (e) Hump-shaped, (f) concave waved (Fig. 3). From 2001 to 2014, the type of boundary lines was consistently negative linear (Fig. 6). The constraint lines below the boundary lines have different line types, but there are not many differences in the SL distribution range (Fig. 6). Interestingly, the distributions of the constraint lines extracted from the 60 % – 99.99 % quantiles were relatively sparse, with clear and distinct line patterns, and the boundary lines were much higher than 90 % constraint lines (Fig. 5). In contrast, the constraint lines below 60 % were more densely distributed and mainly located in the 0–5 kg/m^2 range of SL (Fig. 5). Despite the different line types, they appeared almost the same in the overall bivariate scatter plot view. As NPP gradually increased, SL on all the constraint lines eventually tended to zero. Generally, the lower the quantile by which the constraint line was extracted, the smaller the NPP was when its SL tended to zero (Fig. 5).

3.3. Eigenvalues of constraint lines

The eigenvalues of the boundary lines and lower quantile constraint lines were analyzed separately. The boundary points could be fitted to primary linear equations with higher R^2, so we used primary linear equations and extract its eigenvalues to get the simplest relationship between NPP and SL The slope (k) and intercept (b) were extracted as eigenvalues, and for the lower quantile constraint lines, on the primary linear equations fitted to the boundary points, and the threshold, i.e., the point with the largest change in the curve, was extracted as an eigenvalue on the lower quantile constraint lines. At the same time, because the 50 % and lower quantile constraint lines were denser and more

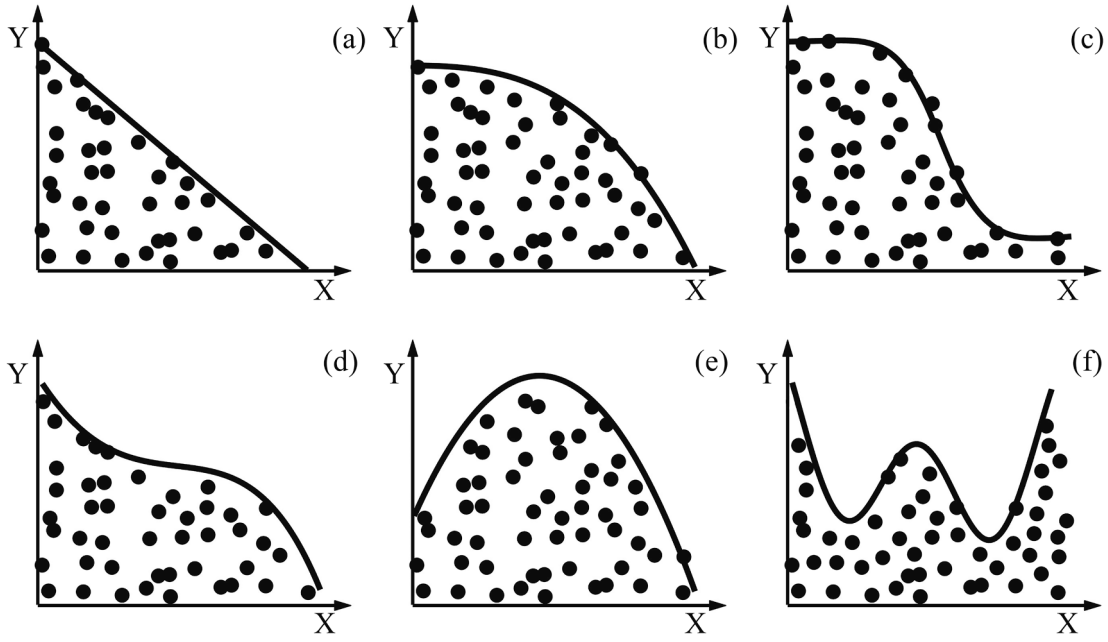

Fig. 3. The types of the constraint lines between NPP and SL.

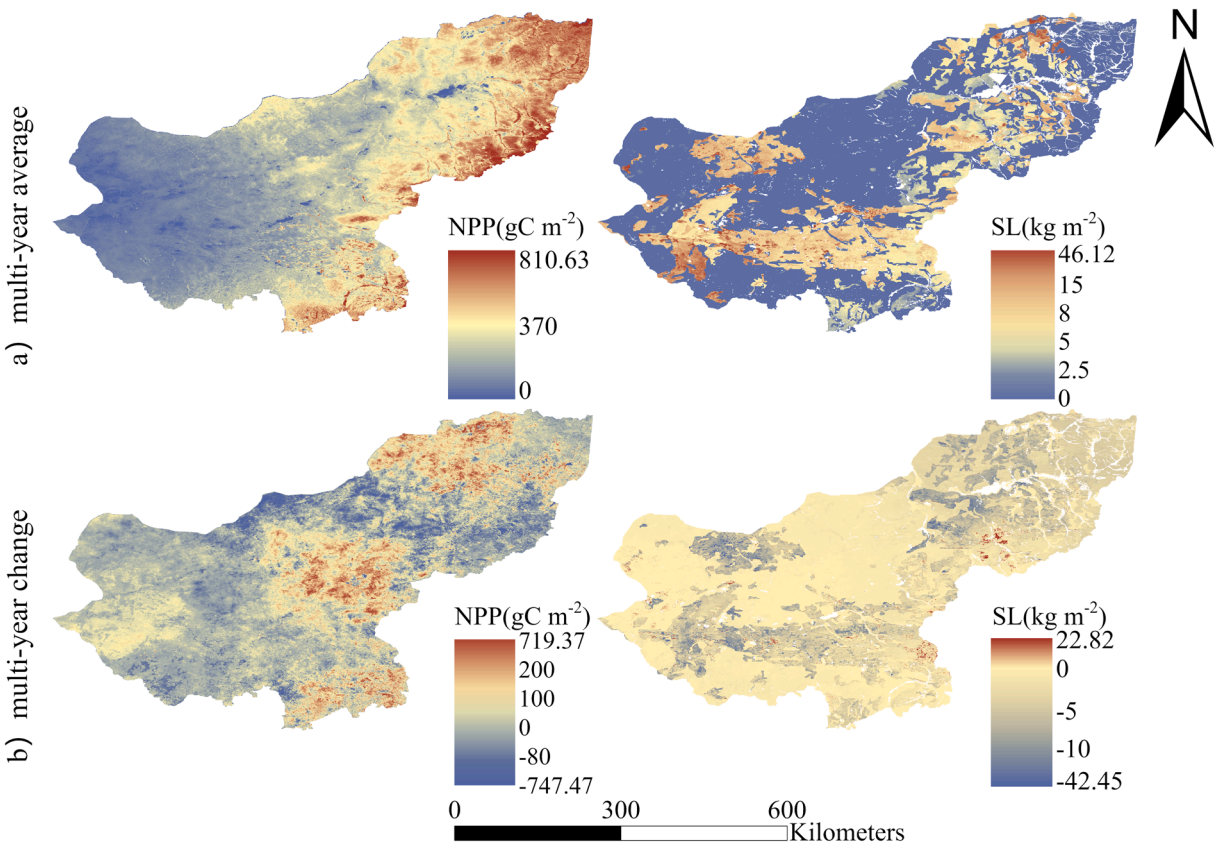

Fig. 4. Spatial distribution and temporal variation of NPP and SL in the Xilin Gol League.

cluttered, which had no mathematical significance, the eigenvalues were not extracted.

3.3.1. *Eigenvalues of linear constraint lines*

Table 2 provides the slopes (k) and intercepts (b) of the primary linear equations for each year. k represents the capacity of NPP to constrain SL, with lower values of k indicating a stronger capacity for the constraint. b represents the number of SL when NPP is 0 gC/m^2, i.e., the value that soil wind erosion will reach when there was no vegetation to constrain soil wind erosion. During the study period, both k and b showed no obvious trend of variation, and it was relatively stable over a large time scale. From 2001 to 2014, NPP has always had a strong and stable linear constraint effect on SL.

3.3.2. *Eigenvalues of nonlinear constraint lines*

Fig. 7 provides the thresholds for the non-linear constraint lines in the Xilin Gol League. The thresholds of the constraint lines mainly appeared in the constraint lines of 60 % and higher, and few thresholds on the constraint lines of lower quantile value were extracted. The thresholds extracted from the 60 % and above quantile non-linear constraint lines showed different patterns at different scales, such as the ranges and the number of thresholds for different years.

The medians of SL corresponding to the thresholds of the different quantile constraint lines showed a steady increasing trend with the increase in quantile, but the change range tended to widen. Many outliers appeared on the 70 % quantile constraint lines (Fig. 8). The medians of NPP thresholds for the different quantile constraint lines were stable between 250 gC/m^2 and 400 gC/m^2. The change range was mainly between 200 gC/m^2 and 400 gC/m^2 (Fig. 9). More specifically, in all of the 63 thresholds extracted, the NPP values ranged from 60 gC/m^2 to 610 gC/m^2, and in the 31 thresholds, i.e., almost half of the thresholds, NPP values were in the range of 250–450 gC/m^2. In addition, the largest number of thresholds (6) are concentrated in the interval 290–310 gC/m^2, followed by the number of thresholds (4 each) in the ranges 270–290 gC/m^2 and 390–410 gC/m^2. This showed that 300 gC/m^2 and 400 gC/m^2 represent the two main concentration points for the thresholds occurring around. Additionally, 300 gC/m^2 and 400 gC/m^2 were also the two inflection points on the S-shaped constraint lines between which SL varied to a less extent in the vast majority of cases.

4. Discussion

4.1. *Comparison with relevant studies*

Unlike previous studies that used the constraint line method to study the relationship between vegetation and soil wind erosion (Allgaier, 2008; Buckley, 1987; Dupont et al., 2014), in which only boundary lines were mostly fitted, the constraint lines fitted by the quantiles ranging from 10 % to 99.99 % with an interval of 10 % can mine more ecological information implied within the scatter cloud. We found that the boundary lines were negatively linear (Fig. 6), which was consistent with previous research in the Xilin Gol League (Hao et al., 2019), but there were also studies reporting that NPP has no obvious constraint effect on SL in farmland in northern China and exponential effect in the Xilin Gol League (Hao et al., 2017; Li et al., 2021). This discrepancy might be attributed to different land use types and the spatial scales.

The constraint lines below the boundary lines showed considerable variation in terms of line type (Fig. 6). In an ideal scenario, the response variable should be influenced only by the limiting variable, so both related variables would distribute around a line (i.e., boundary lines) (Guo et al., 1998). However, in reality, factors other than the limiting variable also have a constraint effect on the response variable. As a result, these points will distribute below the line (Cade and Noon, 2003). The number and strength of factors other than the limiting variable determine the point distribution. The more factors there are and the stronger their constraint, the further the points are from the boundary

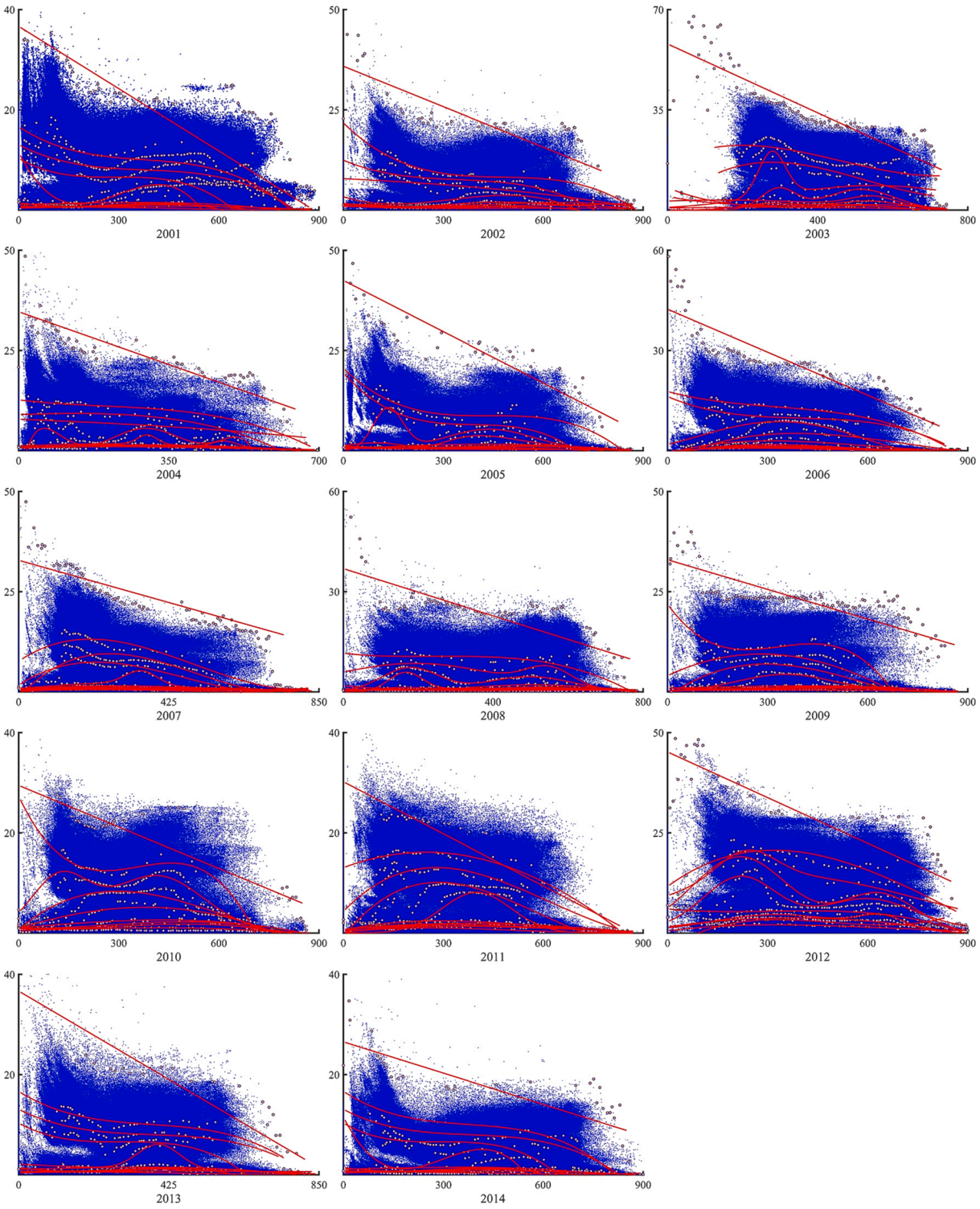

Fig. 5. Scatter plots (blue dots), boundary points (pink dots), and constraint lines (red lines). NPP (gC/m^2) is in the X-axis and SL (kg/m^2) is in the Y-axis. (For interpretation of the references to colour in this figure legend, the reader is referred to the web version of this article.)

line. The varying type of the constraint lines fitted by these points reflected the influence of multiple factors on SL in complex ecosystem, though it is difficult to sort every factor to identify their effects. It can be suggested that the coupling effect of these factors to constrain SL is unstable. The constraint lines fitted by 50 % and lower quantiles distributed densely and ranged from about 0–5 kg/m^2 (Fig. 5), indicating that SL is within this range in nearly half of the study area. Moreover, since SL below the 50 % constraint lines did not change much in any range of NPP (Fig. 5), it can be assumed that SL in these areas is largely constrained by factors other than vegetation. In prior studies, factors such as soil texture (Fryrear et al., 1994) and weather factors (i.e., precipitation, temperature, and wind speed) (Zhao et al., 2017a) have been shown to influence soil wind erosion. Without describing these constraint lines below the boundary lines, it is probable to be confused that the points are uniformly distributed in the scatter cloud and thus miss this feature.

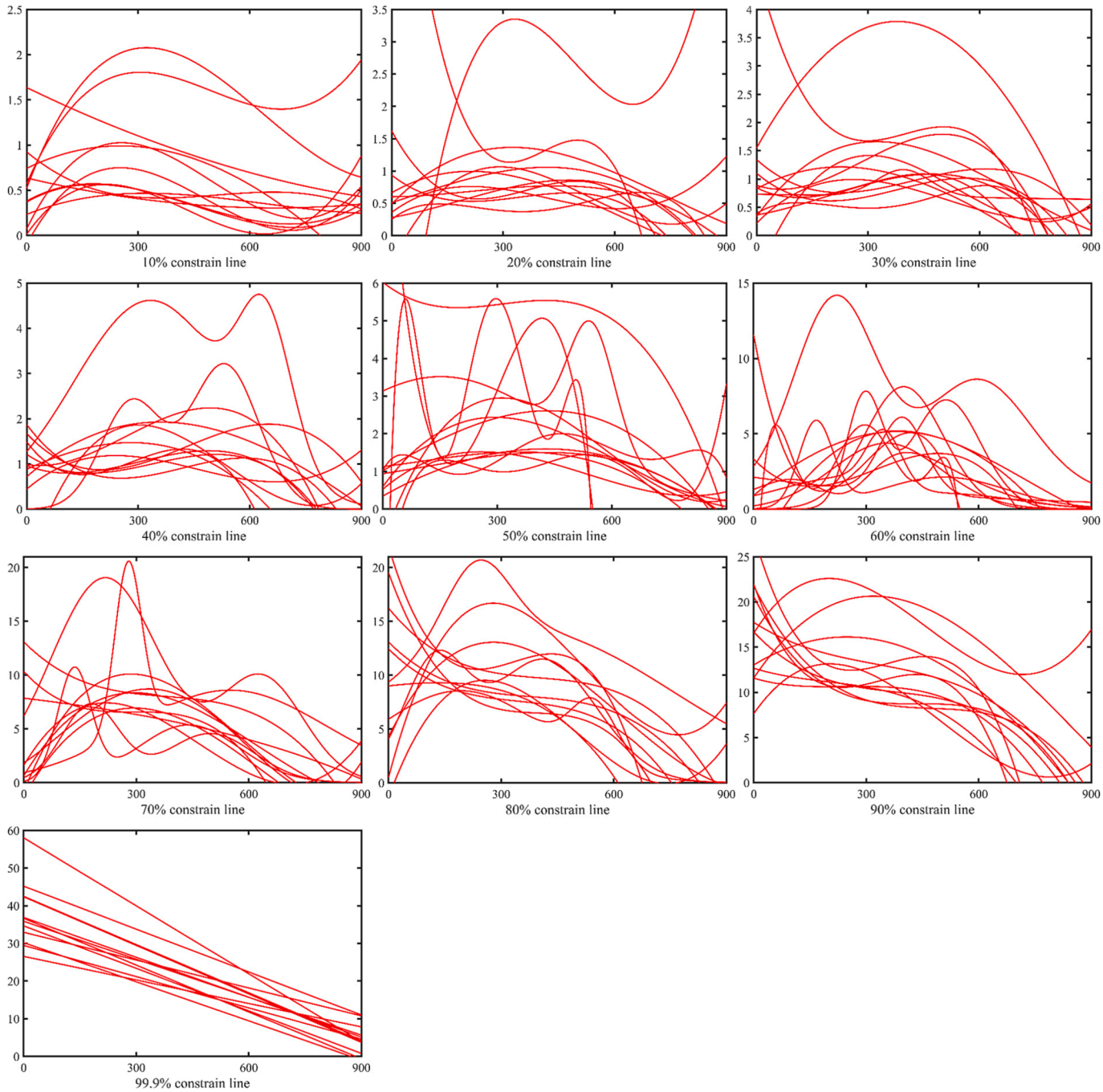

Fig. 6. Constraint line of NPP (gC/m^2) in the X-axis and SL (kg/m^2) in the Y-axis by quantile.

Threshold related analysis is the focus of this study, but unlike other studies (Hao et al., 2017), we extracted the thresholds for multi-scale constraint lines. The number of thresholds obtained was larger and the time scale was longer, so the occurrence range of the thresholds obtained may be more reliable. In the grassland region, similar to other studies, the boundary constraint effect of NPP on SL featured a negative linear relationship with a high R^2, i.e., SL simply decreased with increasing NPP. This study found that the thresholds the internal quantile lines were mainly at the two inflection points of the S-shape, which indicated that when NPP was less than the first threshold, an increase in NPP had a significant and decreased constraint effect on SL. However, when the NPP value was between the two thresholds, the constraint effect of NPP on SL was very limited. When NPP was greater than the second threshold, NPP again had a significant constraint effect on SL.

4.2. *The underlying mechanisms of the NPP-SL constraint lines*

Vegetation plays a crucial role in protecting soils from erosion by increasing surface roughness, reducing the erosive force of precipitation, and absorbing the downward momentum of the ambient air stream (Li et al., 2005; Wasson and Nanninga, 1986). Additionally, the belowground parts of vegetation improve soil stability and reduce the scouring effects of runoff (Shi et al., 2004). Overall, the vegetation provides a multifaceted defense against soil erosion. Thus, the boundary lines of NPP-SL scatter clouds were shaped as negative linear (Fig. 6).

Below the boundary lines, the distribution of the points was not only determined by the limiting variable but also others (Thomson et al.,

Table 2
Slopes (k) and constant (b) of the primary linear equations in the Xilin Gol League.

Year	Slope (k)	Intercept (b)
2001	−0.025	32.82
2002	−0.034	35.87
2003	−0.060	58.02
2004	−0.038	34.66
2005	−0.043	42.48
2006	−0.043	42.36
2007	−0.025	32.82
2008	−0.035	36.89
2009	−0.025	32.96
2010	−0.028	29.46
2011	−0.035	30.20
2012	−0.038	45.18
2013	−0.041	36.66
2014	−0.021	26.53
Mean value	−0.035	36.92
Standard deviation	0.010	8.03
Coefficient of variation	0.29	0.23
Trend	+	−

* Trend of + indicates an upward trend for the data group, while − indicates a downward trend.

1996). For instance, assuming that SL is affected almost exclusively by NPP, the SL values should be concentrated around the b values in the boundary line equations when NPP approaches 0 gC/m^2. However, the reality is that in most years, when NPP is in the range of approximately 0–100 gC/m^2, SL is concentrated in the range of 0–5 kg/m^2 (Fig. 5), which may be due to the lack of existing topsoil in thin vegetated areas. In the areas where NPP is slightly higher than this range, sufficient existing topsoil and sparse spacing between plants cause the "funnel effect" (winds tend to speed up as they squeeze through gaps of sparse plants), which increases surface wind speed and intensifies soil wind erosion, resulting in some constraint lines showing hump-shaped or concave waved. The constraint lines can reveal the quantity and intensity of factors that influence soil wind erosion. We believe that constraint lines at 90 % and 50 % quantiles are more noteworthy: if the relative distance between the 90 % constraint lines and boundary lines is larger, or the initial SL value for the 90 % constraint line is almost half or less than the initial value for the boundary line (Fig. 5), the soil wind erosion is mainly constrained by vegetation and less by the rest of the factors in only a small portion of the study area, while SL in the vast majority of the area is affected by multiple factors. This is consistent with the fact that a single variable is more susceptible to multivariate effects in complex ecosystems such as grasslands (Guo and Rundel, 1998). The constraint lines at 50 % and below quantiles distribute extremely densely, and soil wind erosion is concentrated in the 0–5 kg/m^2 range (Fig. 5), which not only provides information that soil wind erosion is in the 0–5 kg/m^2 range in nearly half of the region, but also indicates that the positive effect of factors other than vegetation on soil wind erosion control should not be neglected as well.

By analyzing the threshold values on the different quantile constraint lines, we found a more specific constraint mechanism of NPP-SL, namely the existence of a "constraint bottleneck". A "constraint bottleneck" means that an increase in NPP cannot constrain a decrease in SL for a certain period of time, resulting in a situation where SL is not constrained by NPP or even increases. The existence of "constraint bottleneck" means that the protection and enhancement of NPP in the greening projects does not always have a constraint effect on SL. Additionally, the "constraint bottleneck" must be considered from the other side. SL is in its most stable phase when NPP is in the "constraint bottleneck" phase, therefore, SL would not increase even if NPP decreases. When implementing practical engineering measures, we need to consider using or avoiding the "constraint bottleneck" period in relation to the actual situation.

4.3. Implications of the constraint line method for grassland ecosystem management

To reduce soil erosion and improve ecosystem service, the Chinese government has implemented large-scale grassland restoration policies

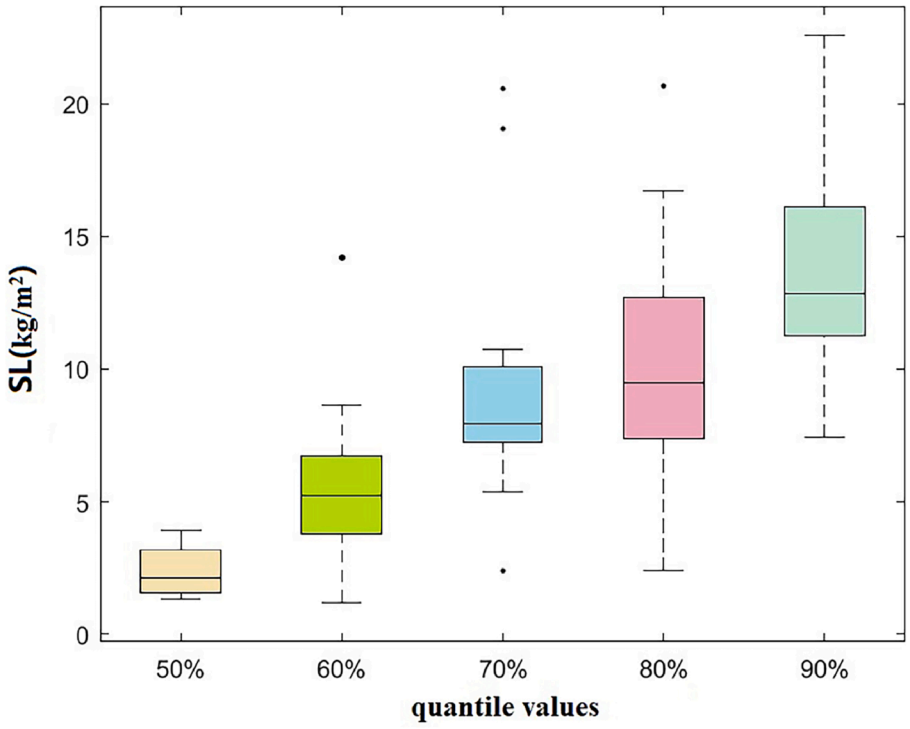

Fig. 7. Box plot of non-linear constraint line thresholds, with horizontal coordinates for the different quantiles and vertical coordinates for the SL value corresponding to the thresholds present on the constraint lines (SL unit: kg/m^2).

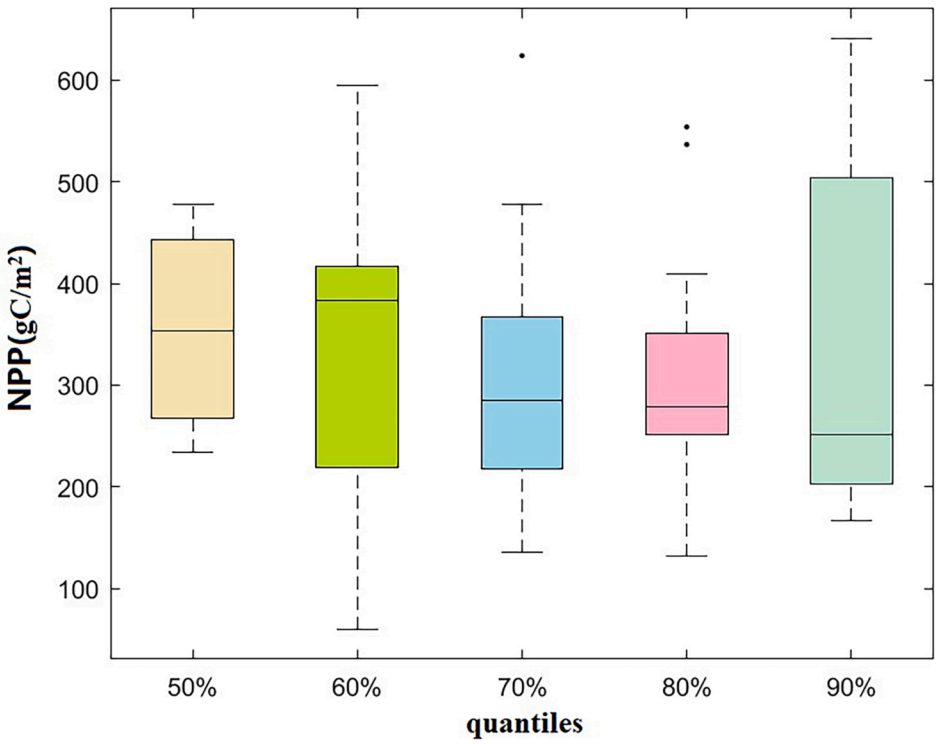

Fig. 8. Box plots of the thresholds on the non-linear constraint lines, with horizontal coordinates for the different quantiles and vertical coordinates for the NPP thresholds (gC/m^2).

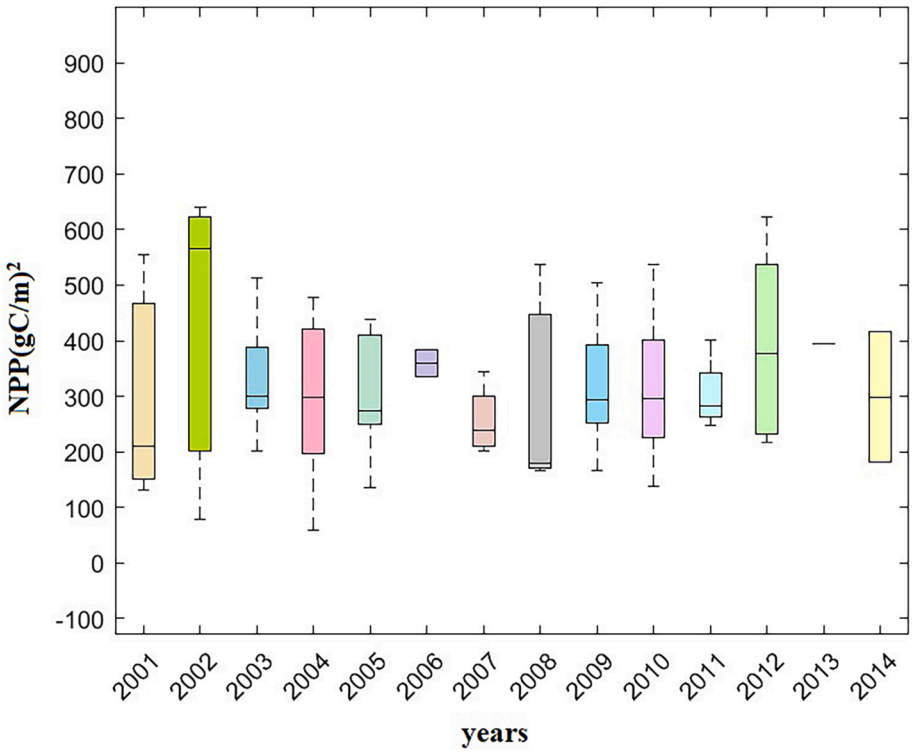

Fig. 9. Box plot of the thresholds on the non-linear constraint lines, with horizontal coordinates for different years and vertical coordinates for the NPP thresholds (gC/m^2).

in Xilin Gol, which have met with success, but these policies still have the potential to optimize (Wu et al., 2015). According to the Standards for classification and gradation of soil erosion issued by the Ministry of Water Resources of the People's Republic of China, the wind erosion intensity in the range of 0–2.5 kg/m^2 is slight and mild, which occupies more than half of Xilin Gol, including many areas with low NPP. This situation prompts policy makers to pay integrated attention to and utilize all factors in the region that are beneficial for controlling soil wind

erosion. Although the constraint lines showed that soil wind erosion eventually tends to disappear with increasing NPP, policy makers should not blindly increase NPP. If the improvement of NPP is significant, it may be ineffective for soil wind erosion due to the existence of "constraint bottleneck", resulting in a waste of human and financial resources. Meanwhile, a significant increase in NPP may not be beneficial to the local ecosystem either. Previous studies have mentioned that when NPP exceeds a certain threshold, water-related ecosystem services may decrease rapidly (Cao et al., 2018; Hao et al., 2022). These thresholds deserve special attention when controlling soil wind erosion through vegetation and NPP should be avoided to exceed them to prevent mutations of other variables. In the view of the previous studies conducted in the same study area (Hao et al., 2019; Li et al., 2021), although the optimal vegetation conditions vary across the study area, we believe that maintaining the NPP in the range of 500–600 gC/m^2 is more conducive to achieve a win-win situation.

The constraint line method is a powerful tool for studying the relationships between variables in the complex ecosystems. This study explores the in-depth application of the constraint-line method in ecology. However, the constraint line method still has its limitations. Since the constraint effect of NPP on SL is scale-dependent and context-dependent (Hao et al., 2017), whether the research results can be extrapolated to other regions remains to be thoroughly investigated. For example, there is not yet a well-developed method to combine the point distribution in the scatter clouds with their spatial distribution characteristics, and this combination may also be informative for ecology. In the future, the integration of constraint lines with different analytical tools should be promoted to facilitate our understanding of the relationships between ecological variables and the associated ecological mechanisms.

5. Conclusions

In this study, by estimating NPP and SL for the period 2001–2014 in the Xilin Gol League, the NPP-SL scatter cloud data was analyzed in depth for further explaining the constraint effect of NPP on SL. Importantly, the paper uncovered the rich ecological meanings contained within the scatter clouds, and the multi-quantile constraint lines proved to be an effective method to use the scatter cloud datasets.

By fitting different quantiles of NPP and SL, we found a significant difference in the density of constraint lines above the 60 % quantile and below the 50 % quantile, indicating that even with great spatial heterogeneity in vegetation condition, soil wind erosion has remained stable at very low levels over almost half of the study area. We also found that the shape of the constraint lines was predominantly S-shaped, suggesting the existence of a "constraint bottleneck" interval with characteristic range to guide greening behaviors aimed at reducing soil wind erosion. The negative constraint effect of NPP on SL was confirmed based on an extension of the constraint line method, and it showed that other ecological factors were more likely to disrupt this constraint effect when SL was at the lower half of the scatter clouds. This finding provides theoretical support for wind erosion resistance in the Xilin Gol League and indeed all arid and semi-arid region.

Declaration of Competing Interest

The authors declare that they have no known competing financial interests or personal relationships that could have appeared to influence the work reported in this paper.

Data availability

The data that has been used is confidential.

Acknowledgments

This research was supported by the Program of National Natural Science Foundation of China [grant number 42001260].

References

Akiyama, T., Kawamura, K., 2007. Grassland degradation in China: Methods of monitoring, management and restoration. Grassland Science 53, 1–17. https://doi.org/10.1111/j.1744-697X.2007.00073.x.

Ali, I., Cawkwell, F., Dwyer, E., Barrett, B., Green, S., 2016. Satellite remote sensing of grasslands: from observation to management. Journal of Plant Ecology 9, 649–671. https://doi.org/10.1093/jpe/rtw005.

Allgaier A., 2008. Aeolian Sand Transport and Vegetation Cover. 211-224.

Bengtsson, J., Bullock, J.M., Egoh, B., Everson, C., Everson, T., O'Connor, T., O'Farrell, P. J., Smith, H.G., Lindborg, R., 2019. Grasslands—more important for ecosystem services than you might think. Ecosphere 10, e02582. https://doi.org/10.1002/ecs2.2582.

Buckley, R., 1987. The effect of sparse vegetation on the transport of dune sand by wind. Nature 325, 426–428. https://doi.org/10.1038/325426a0.

Cade, B., Noon, B., 2003. A Gentle Introduction to Quantile Regression for Ecologists. Frontiers in Ecology and the Environment 1, 412–420. https://doi.org/10.1890/1540-9295(2003)001[0412:AGITQR]2.0.CO;2.

Cao, Z., Li, Y., Liu, Y., Chen, Y., Wang, Y., 2018. When and where did the Loess Plateau turn "green"? Analysis of the tendency and breakpoints of the normalized difference vegetation index. Land Degradation & Development 29, 162–175. https://doi.org/10.1002/ldr.2852.

Dupont, S., Bergametti, G., Simoëns, S., 2014. Modelling Aeolian Erosion in Presence of Vegetation. Journal of Geophysical Research: Earth Surface 119. https://doi.org/10.1002/2013JF002875.

Fryrear, D.W., Krammes, C.A., Williamson, D.L., Zobeck, T.M., 1994. Computing the wind erodible fraction of soils. Journal of Soil & Water Conservation 49, 183–188.

Fryrear, D., Saleh, A., Bilbro, J., 1998. A single event wind erosion model. Transactions of the ASAE 41, 1369–1374. https://doi.org/10.13031/2013.17310.

Gibbens, R., Tromble, J., Hennessy, J., Cardenas, M., 1983. Soil Movement in Mesquite Dunelands and Former Grasslands of Southern New Mexico from 1933 to 1980. Journal of Range Management 36, 145. https://doi.org/10.2307/3898148.

Gong, G., Liu, J., Shao, Q., 2014a. Wind erosion in Xilingol League, Inner Mongolia since the 1990s using the Revised Wind Erosion Equation. PROGRESS IN GEOGRAPHY 33, 825–834. https://doi.org/10.11820/dlkxjz.2014.06.011.

Gong, G., Liu, J., Shao, Q., Zhai, J., 2014b. Sand-Fixing Function under the Change of Vegetation Coverage in a Wind Erosion Area in Northern China. Journal of Resources and Ecology 5, 105–114. https://doi.org/10.5814/j.issn.1674-764x.2014.02.002.

Guo, Q., Brown, J., Enquist, B., 1998. Using Constraint Lines to Characterize Plant Performance. Oikos 83, 237–245. https://doi.org/10.2307/3546835.

Guo, Q., Rundel, P.W., 1998. SELF-THINNING IN EARLY POSTFIRE CHAPARRAL SUCCESSION: MECHANISMS, IMPLICATIONS, AND A COMBINED APPROACH. Ecology 79, 579–586. https://doi.org/10.1890/0012-9658(1998)079[0579:STIEPC]2.0.CO;2.

Guo, Z., Zobeck, T., Zhang, K., Li, F., 2013. Estimating potential wind erosion of agricultural lands in northern China using the Revised Wind Erosion Equation and geographic information systems. Journal of Soil and Water Conservation 68, 13–21. https://doi.org/10.2489/jswc.68.1.13.

Han, Y., Zhou, A., Pereira, P., 2023. Water and wind erosion response to ecological restoration measures in China's drylands. Geoderma 435, 116514. https://doi.org/10.1016/j.geoderma.2023.116514.

Hao, R., Yu, D., Wu, J., Guo, Q., Liu, Y.P., 2016. Constraint line methods and the applications in ecology. Chinese Journal of Plant Ecology 40, 1100.

Hao, R., Yu, D., Wu, J., 2017. Relationship between paired ecosystem services in the grassland and agro-pastoral transitional zone of China using the constraint line method. Agriculture, Ecosystems & Environment 240, 171–181. https://doi.org/10.1016/j.agee.2017.02.015.

Hao, R., Yu, D., Sun, Y., Shi, M., 2019. The features and influential factors of interactions among ecosystem services. Ecological Indicators 101, 770–779. https://doi.org/10.1016/j.ecolind.2019.01.080.

Hao, R., Yu, D., Huang, T., Li, S., Qiao, J., 2022. NPP plays a constraining role on water-related ecosystem services in an alpine ecosystem of Qinghai. China. Ecological Indicators 138, 108846. https://doi.org/10.1016/j.ecolind.2022.108846.

Hou, L., Xia, F., Chen, Q., Huang, J., He, Y., Rose, N., Rozelle, S., 2021. Grassland ecological compensation policy in China improves grassland quality and increases herders' income. Nature Communications 12, 4683. https://doi.org/10.1038/s41467-021-24942-8.

Hu, M., Liu, Y., Wu, L., Yang, Z., Wu, D., Wang, G., 1991. A Experimemtal StUdy in Wind Tunnel on Wind Erosion of Soil in Korqin Sandy Land. Journal of Desert Research 11, 22–29.

Hui, J., Chen, Z., ye, B., Shi, C., Bai, Z., 2022. Remote Sensing Monitoring of the Spatial Pattern of Greening and Browning in Xilin Gol Grassland and Its Response to Climate and Human Activities. Remote Sensing 14, 1765. https://doi.org/10.3390/rs14071765.

Kang, L., Han, X., Zhang, Z., Sun, O.J., 2007. Grassland ecosystems in China: review of current knowledge and research advancement. Philosophical Transactions of the Royal Society of London. Series B, Biological Sciences 362, 997–1008. https://doi.org/10.1098/rstb.2007.2029.

Li, F.R., Kang, L.F., Zhang, H., Zhao, L.Y., Shirato, Y., Taniyama, I., 2005. Changes in intensity of wind erosion at different stages of degradation development in grasslands of Inner Mongolia, China. Journal of Arid Environments 62, 567–585. https://doi.org/10.1016/j.jaridenv.2005.01.014.

Li, J., Li, Z., Guo, M., Li, P., Cheng, S., Yuan, B., 2018. Effects of vegetation restoration on soil physical properties of abandoned farmland on the Loess Plateau. China. Environmental Earth Sciences 77, 205. https://doi.org/10.1007/s12665-018-7385-7.

Li, S., Li, X., Huashun, D., Dang, D., Gong, J., 2021. Integrating constraint effects among ecosystem services and drivers on seasonal scales into management practices. Ecological Indicators 125, 107425. https://doi.org/10.1016/j.ecolind.2021.107425.

Liu, W., Zhang, B., Wang, Z., Song, K., Liu, D., Ren, C., Du, J., 2010. Development of a GIS-based decision support system for eco-environment and natural resources of Northeast Asia. Energy Policy - ENERG POLICY 2, 906–913. https://doi.org/10.1016/j.proenv.2010.10.102.

Potter, C., Randerson, J., Field, C., Matson, P., Vitousek, P., Mooney, H., Klooster, S., 1993. Terrestrial Ecosystem Production: A Process Model Based on Global Satellite and Surface Data. Global Biogeochemical Cycles 7, 811–841. https://doi.org/10.1029/93GB02725.

Shang, R., Qi, Y., Zhao, T., Ding, G., 2006. Field investigation on the influence of vegetation on wind and soil erosion. Research of Soil and Water Conservation 13, 37–39.

Shao, L., Chen, H., Zhang, C., Huo, X., 2017. Effects of Major Grassland Conservation Programs Implemented in Inner Mongolia since 2000 on Vegetation Restoration and Natural and Anthropogenic Disturbances to Their Success. Sustainability 9, 466. https://doi.org/10.3390/su9030466.

Shi, Z.H., Cai, C.F., Ding, S.W., Wang, T.W., Chow, T.L., 2004. Soil conservation planning at the small watershed level using RUSLE with GIS: a case study in the Three Gorge Area of China. Catena 55, 33–48. https://doi.org/10.1016/S0341-8162(03)00088-2.

Siddoway, F., Chepil, W., Armbrust, D., 1965. Effect of Kind, Amount, and Placement of Residue on Wind Erosion Control. Transactions of the ASAE 8. https://doi.org/10.13031/2013.40507.

Sun, B., Li, Z., Gao, Z., Guo, Z., Wang, B., Hu, X., Bai, L., 2017. Grassland degradation and restoration monitoring and driving forces analysis based on long time-series remote sensing data in Xilin Gol League. Acta Ecologica Sinica 37, 219–228. https://doi.org/10.1016/j.chnaes.2017.02.009.

Thomson, J.D., Weiblen, G., Thomson, B.A., Alfaro, S., Legendre, P., 1996. Untangling Multiple Factors in Spatial Distributions: Lilies, Gophers, and Rocks. Ecology 77, 1698–1715. https://doi.org/10.2307/2265776.

Tian, M., Gao, J., Zhang, L., Zhang, H., Feng, C., Jia, X., 2021. Effects of dust emissions from wind erosion of soil on ambient air quality. Atmospheric Pollution Research 12, 101108. https://doi.org/10.1016/j.apr.2021.101108.

Wang, S., Zhang, B., Xie, G.-D., Zhai, X., Sun, H.-L., 2020. Vegetation cover changes and sand-fixing service responses in the Beijing-Tianjin sandstorm source control project area. Environmental Development 34, 100455. https://doi.org/10.1016/j.envdev.2019.08.002.

Wasson, R.J., Nanninga, P.M., 1986. Estimating wind transport of sand on vegetated surfaces. Earth Surface Processes and Landforms 11, 505–514. https://doi.org/10.1002/esp.3290110505.

Wu, J., Zhang, Q., Li, A., Liang, C., 2015. Historical landscape dynamics of Inner Mongolia: patterns, drivers, and impacts. Landscape Ecology 30, 1579–1598. https://doi.org/10.1007/s10980-015-0209-1.

Yan, Y., Xu, X., Xin, X., Yang, G., Wang, X., Yan, R., Chen, B., 2011. Effect of vegetation coverage on aeolian dust accumulation in a semiarid steppe of northern China. Catena 87, 351–356. https://doi.org/10.1016/j.catena.2011.07.002.

Zhang, M., Lal, R., Zhao, Y., Jiang, W., Chen, Q., 2016. Estimating net primary production of natural grassland and its spatio-temporal distribution in China. Science of the Total Environment 553, 184–195. https://doi.org/10.1016/j.scitotenv.2016.02.106.

Zhang, B., Xiong, D., Liu, L., Tang, Y., 2022. Wind erodibility indices of aeolian sandy soils impacted by different vegetation restoration: a case study from the Shannan valley of the Yarlung Zangbo River. Journal of Mountain Science 19, 2830–2845. https://doi.org/10.1007/s11629-022-7305-x.

Zhang, Y., Xu, D., Wang, Z., Zhang, X., 2021. The interaction of driving factors for the change of windbreak and sand-fixing service function in Xilingol League between 2000 and 2015. Acta Ecol. Sinica 41, 603–614.

Zhao, G., Mu, X., Jiao, J., An, Z., Klik, A., Wang, F., Jiao, F., Yue, X., Gao, P., Sun, W., 2017a. Evidence and Causes of Spatiotemporal Changes in Runoff and Sediment Yield on the Chinese Loess Plateau. Land Degradation & Development 28, 579–590. https://doi.org/10.1002/ldr.2534.

Zhao, Y., Wu, J., He, C., Ding, G., 2017b. Linking wind erosion to ecosystem services in drylands: a landscape ecological approach. Landscape Ecology 32, 2399–2417. https://doi.org/10.1007/s10980-017-0585-9.

Zhu, W.Q., Pan, Y., Zhang, J.S., 2007. Estimation of net primary productivity of Chinese terrestrial vegetation based on remote sensing. Journal of Plant Ecology 31, 413–424. https://doi.org/10.17521/cjpe.2007.0050.